DOI:10.1021/ic900329w

Inorganic Chemistry
Article

# Nickelacyclic-Cobaltocene vs. Nickelacyclic-Nickelocene. Synthesis, X-ray Structures, Electron Transfer Activity, EPR Spectroscopy, and Theoretical Calculations

**Piotr Buchalski,*,† Elbieta Kamińska,† Katarzyna Piwowar,† Kinga Suwińska,‡ Lucjan Jerzykiewicz,§ Fulvio Rossi,# Franco Laschi,# Fabrizia Fabrizi de Biani,# and Piero Zanello*,#**

†*Faculty of Chemistry, Warsaw University of Technology, Koszykowa 75, 00-662 Warsaw, Poland,* ‡*Institute of Physical Chemistry of the Polish Academy of Sciences, Kasprzaka 44/52, 01-224 Warsaw, Poland,* §*Faculty of Chemistry, University of Wrocław, Joliot-Curie 14, 50-353 Wrocław, Poland, and* #*Dipartimento di Chimica, Università di Siena, Via De Gasperi, 2, 53100 Siena, Italy*

Received February 18, 2009

Reactions of 9-nickelafluorenyllithium with cobalt and nickel pentamethylcyclopentadienyl-acetylacetonates resulted in the formation of the novel nickelacyclic-cobaltocene **2** and nickelacyclic-nickelocene **3**, respectively, in which the central metal atom is bonded to the nickelafluorenyl ring. On the basis of their redox propensity, compounds **2** and **3** were oxidized to the corresponding monocations $[\mathbf{2}]^+$ and $[\mathbf{3}]^+$. The crystal and molecular structures of both the redox couples were determined by single-crystal X-ray analysis. In spite of their structural similarity, they display a rather different electron transfer ability. To throw light on such an aspect, the pertinent redox couples have been examined by EPR spectroscopy and the nature of the frontier orbitals involved in the redox activity of the neutral precursors has been supported by extended Hckel theoretical calculations.

## Introduction

Metallametallocenes are the compounds in which one or two cyclopentadienyl groups of metallocene are replaced by a metallacyclopentadienyl ring, Scheme 1.[1]

In previous papers, we described the synthesis of a few nickelametallocenes[2] that possessed one nickelaindenyl or nickelafluorenyl ring, together with their electrochemical properties.[3] More recently, we have employed 9-nickelafluorenyllithium, **1**,[4] in the synthesis of the first analogues of nickelocene and cobaltocene with two nickelafluorenyl rings.[5] In the present paper, we describe the synthesis of metallacobaltocenes **2** and that of the monocations $[\mathbf{2}]^+$ and $[\mathbf{3}]^+$, Chart 1

## Experimental Section

All reactions were carried out in an atmosphere of dry argon or nitrogen using Schlenk tube techniques. Solvents were dried by conventional methods. $^1$H and $^{13}$C NMR spectra were measured on a Varian Mercury 400BB instrument. Electron Impact mass spectra were recorded on an

* To whom correspondence should be addressed. E-mail: pjb@ch.pw.edu.pl (P.B.); zanello@unisi.it (P.Z.).

(1) See for example(a) Baimbridge, C. W.; Dickson, R. S.; Fallon, G. D.; Grayson, I.; Nesbit, R. J.; Weigold, J. *Aust. J. Chem.* **1986**, *39*, 1187. (b) McGhee, W. D.; Bergman, R. G. *J. Am. Chem. Soc.* **1988**, *110*, 4246. (c) Sünkel, K. *J. Organomet. Chem.* **1990**, *391*, 247.dPerthuisot, C.; Edelbach, B. L.; Zubris, D. L.; (e) Omori, H.; Suzuki, H.; Moro-oka, Y. *Organometallics* **1989**, *8*, 1576. (f) Campion, B. K.; Heyn, R. H.; Tilley, T. D. *Organometallics* **1990**, *9*, 1106. (g) Luo, S.; Ogilvy, A. E.; Rauchfuss, T. B.; Rheingold, A. L.; Wilson, S. R. *Organometallics* **1991**, *10*, 1002. (h) Brady, L. A.; Dyke, A. F.; Garner, S. E.; Knox, S. A. R.; Irving, A.; Nicholls, S. M.; Orpen, A. G. *J. Chem. Soc., Dalton Trans.* **1993**, 487. (i) Suzuki, H.; Omori, H.; Lee, D. H.; Yoshida, Y.; Fukushima, M.; Tanaka, M.; Moro-oka, Y. *Organometallics* **1994**, *13*, 1129. (j) Nishio, M.; Matsuzaka, H.; Mizobe, Y.; Tanase, T.; Hidai, M. *Organometallics* **1994**, *13*, 4214. (k) Wadepohl, H.; Borchert, T.; Büchner, K.; Herrmann, M.; Paffen, F.-J.; Pritzkow, H. *Organometallics* **1995**, *14*, 3817. (l) Jones, W. D. *Organometallics* **1997**, *16*, 2016. (m) Müller, J.; Akhnoukh, T.; Escarpa Gaede, P.; Ao-ling, Guo; Moran, P.; Ke, Qiao *J. Organomet. Chem.* **1997**, *541*, 207. (n) Inagaki, A.; Takemon, T.; Tanaka, M.; Suzuki, H. *Angew. Chem., Int. Ed.* **2000**, *39*, 404. (o) Wadepohl, H.; Metz, A.; Pritzkow, H. *Chem.—Eur. J.* **2002**, *8*, 1591. (p) Kumaraswamy, S.; Jalisatgi, S. S.; Matzger, A. J.; Mijanic, O. S.; Volhardt, K. P. C *Angew. Chem., Int. Ed.* **2004**, *43*, 3711. (q) Dennet, J. N. L.; Knox, S. A. R.; Anderson, K. M.; Charmant, J. P. H. *Dalton Trans.* **2005**, 63. (r) Chen, J.; Young, V. G.; Angelici, R. J. *Inorg. Chim. Acta* **2005**, *358*, 1623. (s) Takemoto, S.; Shimadzu, D.; Kamikawa, K.; Matsuzaka, H.; Nomura, R. *Organometallics* **2006**, *25*, 982.

(2) (a) Buchalski, P.; Pietrzykowski, A.; Pasynkiewicz, S.; Jerzykiewicz, L. B. *J. Organomet. Chem.* **2005**, *690*, 1523. (b) Buchalski, P.; Pasynkiewicz, S.; Pietrzykowski, A.; Piłka, A.; Suwińska, K. *Inorg. Chem. Commun.* **2006**, *9*, 375. (c) Buchalski, P.; Kozioł, A.; Pasynkiewicz, S.; Pietrzykowski, A.; Suwińska, K.; Zdziemborska, M. *J. Organomet. Chem.* **2006**, *691*, 4080.

(3) Losi, S.; Rossi, F.; Laschi, F.; Fabrizi de Biani, F.; Zanello, P.; Buchalski, P.; Burakowska, K.; Piwowar, K.; Zbrzezna, J.; Pasynkiewicz, S.; Pietrzykowski, A.; Suwińska, K.; Jerzykiewicz, L. *Inorg. Chem.* **2007**, *46*, 10659.

(4) Buchalski, P.; Grabowska, I.; Kamińska, E.; Suwińska, K. *Organometallics* **2008**, *27*, 2346.

(5) Buchalski, P.; Grabowska, I.; Karaskiewicz, A.; Suwińska, K.; Jerzykiewicz, L. *Organometallics* **2008**, *27*, 3316.


Published on Web 4/30/2009

**Scheme 1**

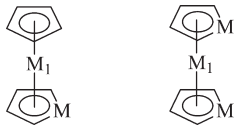


**Chart 1**

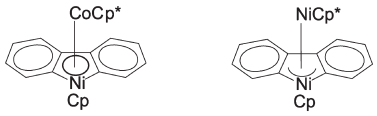


**2** **3**

AMD-604 spectrometer. Electrospray mass spectra were recorded on Applied Biosystems 4000 QTRAP spectrometer. Magnetic susceptibility was determined by NMR measurements at 298 K by Evans method [6] from the differences in the chemical shift of methyl group protons of toluene used as solvent and as external standard. The magnetic moments were calculated from the measurements of magnetic susceptibility. The synthesis of compounds **1**[4] and **3**[7] were described earlier. (Acetylacetonate)(pentamethylcyclopentadienyl)cobalt was synthesized according to the literature.[8]

Electrochemical measurements were performed in deaerated, freshly distilled THF solutions containing $[NBu_4][PF_6]$ (0.2 mol $dm^{-3}$) as supporting electrolyte (Fluka, electrochemical grade). Cyclic voltammetry was performed in a three-electrode cell containing the working electrode surrounded by a platinum-spiral counter electrode and the reference electrode mounted with a Luggin capillary.[9] Platinum or gold electrodes were used as working electrodes. A BAS 100W electrochemical analyzer was used as polarizing unit. All the potential values are referred to the Ag/AgCl electrode. Controlled potential coulometry was performed in an H-shaped cell with anodic and cathodic compartments separated by a sintered/glass disk. The working macroelectrode was a platinum gauze; a mercury pool was used as the counter electrode. Under the present experimental conditions, the one-electron oxidation of ferrocene occurs at +0.54 V.

Extended Hückel calculations were performed using the CACAO98 programs package.[10] Bond distances and angles of the model molecule were taken as the average of the experimental values. Although the MOs energy and composition reported in this work are those obtained using CACAO98, the MOs drawings have been obtained by the software Hyperchem.[11]

Electron spin resonance (ESR) spectra were recorded with a ER 200 D-SRC Bruker spectrometer operating at X-band frequencies using a HS Bruker rectangular cavity. The control of the operational frequency was obtained with a Hewlett-Packard X532B wavemeter, and the magnetic field was calibrated with the DPPH (1,1-diphenyl-2-picrylhydrazyl) radical as a suitable field marker. The temperature was controlled by a Bruker ER 4111 VT device (±1 K) and with an Oxford ESR900 helium continuous-flow cryostat. The *g* values are referred to DPPH ($g = 2.0036$) used as an external standard reference.

**Synthesis of 2.** Compound **1**, 0.329 g (0.88 mmol), and 40 $cm^3$ of diethyl ether were placed in Schlenk flask and cooled to −30 °C. The solution of (acetylacetonate)(pentamethylcyclopentadienyl)cobalt (0.225 g, 0.88 mmol) in 20 $cm^3$ of diethyl ether was slowly added. The reaction was stirred for 1 h at −30 °C, and then at room temperature overnight. After the reaction was completed, white precipitate was allowed to settle. The clear solution was transferred to another Schlenk flask and evaporated to dryness. The black solid was dissolved in 10 $cm^3$ of toluene, filtered, and put in the refrigerator. After 24 h, the solution was removed and the dark solid of **2** was dried under a vacuum (0.237 g, 0.51 mmol, 58%).

EIMS of **2** (70 eV) *m*/*e* (rel. int.) ($^{58}$Ni): 469 (45%, $M^+$), 276 (12%, $C_{17}H_{13}Co^+$), 259 (100%, $C_{15}H_{20}Co^+$), 152 (12%, $C_{12}H_8^+$). EI HR MS: observed, 469.08668; calcd for $C_{27}H_{28}Co^{58}Ni$, 469.08765.

**Oxidation of Complex 2 with $[Cp_2Fe]^+PF_6^-$.** Complex **2**, 0.577 g (1.23 mmol), reacted with $[Cp_2Fe]^+PF_6^-$, 0.400 g (1.23 mmol), in dichloromethane, 40 $cm^3$, at room temperature for 48 h. The resulting dark-green solution was filtered and dried. The resulting black solid was washed three times with diethyl ether and dried. The yield of crude product was 0.442 g (0.72 mmol, 59%). It was then dissolved in dichloromethane and diethyl ether was layered over the solution. After 2 days, crystals of $[\mathbf{2}]^+$ appropriate for X-ray measurements were formed. $^1$H NMR ($CD_2Cl_2$) (25 °C) $\delta$ (ppm): 7.38 − 8.17 (8H, Ar), 5.56 (s, 5H, Cp), 1.31 (s, 15H, Cp*). $^{19}$F NMR ($CDCl_3$) (20 °C) $\delta$ (ppm): −71.19 (d). $^{31}$P NMR ($CDCl_3$) (20 °C) $\delta$ (ppm): −142.88 (septet). Electrospray MS (acetone) *m*/*e* ($^{58}$Ni): 469 ($[\mathbf{2}]^+$), 145 ($PF_6^-$).

**Oxidation of Complex 3 with $[Cp_2Fe]^+PF_6^-$.** Complex **3**, 0.285 g (0.608 mmol), reacted with $[Cp_2Fe]^+PF_6^-$, 0.201 g (0.607 mmol), in dichloromethane 30 $cm^3$ at room temperature for 72 h. The resulting dark-brown solution was filtered and concentrated to 15 $cm^3$. Next, 50 $cm^3$ of diethyl ether was added and a black solid was formed. It was washed three times with diethyl ether and dried. The yield of the crude product was 0.279 g (0.45 mmol, 74%). It was then dissolved in dichloromethane, and diethyl ether was layered over the solution. After 2 days, black crystals of $[\mathbf{3}]^+$ appeared that were appropriate for X-ray measurements. $^1$H NMR ($CD_2Cl_2$) (30 °C) $\delta$ (ppm): 96.26 (s, 15H, Cp*), 10.35 (s, 2H, Ar), 1.71 (s, 2H, Ar), −1.21 (s, 2H, Ar), −4.56 (s, 2H, Ar), −19.00 (s, 5H, Cp), −23.63 (s, 2H, Ar). $^{19}$F NMR ($CDCl_3$) (20 °C) $\delta$ (ppm): −73.86, −75.75. $^{31}$P NMR ($CDCl_3$) (20 °C) $\delta$ (ppm): −142.37. Electrospray MS (acetone) *m*/*e* ($^{58}$Ni): 468 ($[\mathbf{3}]^+$), 145 ($PF_6^-$).

**X-ray Structure Determination of 2.** Preliminary examination and intensities data collections were carried out on a KUMA KM4 $\kappa$-axis diffractometer with graphite-monochromated Mo K$\alpha$ and with CCD camera. All data were corrected for Lorentz, polarization, and absorption effects. Data reduction and analysis were carried out with the Oxford Diffraction programs.[12] The structure was solved by direct methods and refined by the full-matrix least-squares method on all $F^2$ data using the SHELXTL_NT V5.1 software.[13] Carbon-bonded hydrogen atoms were included in calculated positions and refined in the riding mode using SHELXL97 default parameters. Other hydrogen atoms were located in a difference map and refined isotropically without any restrains. All non-hydrogen atoms were refined with anisotropic displacement parameters. The compound crystallizes in the triclinic crystal system. Crystal data, data collection, and refinement parameters for **2** are given in Table 1.

(6) (a) Evans, D. F. *J. Chem. Soc* **1959**, 2003. (b) Crawford, T. H.; Swanson, J. *J. Chem. Educ.* **1971**, *48*, 382.cBraun, S.; Kalinowski, H. O.; Berger, S. *150 and More Basic NMR Experiments*; Wiley-VCH: Weinheim, Germany, 1998.

(7) Buchalski, P.; Kozioł, A.; Suwińska, K. *Acta Crystallogr., Sect. C* **2008**, *64*, m274.

(8) Smith, M. E.; Andersen, R. A. *J. Am. Chem. Soc.* **1996**, *118*, 11119.

(9) Zanello, P. In *Inorganic electrochemistry. Theory, Practice and Application*; Royal Society of Chemistry: Oxford, U.K., 2003.

(10) Mealli, C.; Proserpio, D. M. *J. Chem. Educ.* **1990**, *67*, 390.

(11) *HyperChem(TM) Professional 8.0*; Hypercube, Inc.: Gainesville, FL

(12) *Oxford Diffraction Software, version 1.171.13*; Oxford Diffraction: Yarnton, U.K., 2003.

(13) Sheldrick, G. M. *SHELXTL Version 5.10*; Bruker AXS Inc.: Madison, WI, 1997.

**Table 1.** Crystal Data and Structure Refinement Parameters

| | **2** | **[2]$^+$** | **[3]$^+$** |
|---|---|---|---|
| empirical formula | $C_{27}H_{28}CoNi$ | $C_{27}H_{28}F_6CoNiP$ | $C_{27}H_{28}F_6Ni_2P$ |
| fw | 470.13 | 615.10 | 614.88 |
| $T$ (K) | 100(2) | 150(2) | 100(2) |
| wavelength (Å) | 0.71073 | 0.71073 | 0.71073 |
| cryst syst, space group | rriclinic, $P\bar{1}$ | triclinic, $P\bar{1}$ | triclinic, $P\bar{1}$ |
| $a$ (Å) | 7.462(5) | 8.0275(3) | 8.1653(3) |
| $b$ (Å) | 9.373(6) | 9.1337(4) | 9.0887(3) |
| $c$ (Å) | 15.178(6) | 17.3794(7) | 17.2217(6) |
| α (deg) | 84.71(8) | 85.932(2) | 86.388(2) |
| $\beta$ (deg) | 84.71(8) | 81.788(3) | 81.810(2) |
| $\gamma$ (deg) | 79.13(7) | 79.912(2) | 80.855(2) |
| $V$ (Å$^3$) | 1035(1) | 1240.3(1) | 1247.9(1) |
| $Z$, calcd density (Mg/m$^3$) | 2, 1.508 | 2, 1.647 | 2, 1.636 |
| absorp coeff (mm$^{-1}$) | 1.721 | 1.552 | 1.633 |
| $F$(000) | 490 | 628 | 630 |
| cryst size (mm$^3$) | 0.26 × 0.08 × 0.06 | 0.50 × 0.40 × 0.15 | 0.44 × 0.40 × 0.04 |
| theta range for data collection (deg) | 3.00−26.50 | 3.00−26.34 | 2.91−27.48 |
| limiting indices | $9 \le h \le 9$, $-11 \le k \le 11$, $-19 \le l \le 15$ | $-9 \le h \le 10$, $-11 \le k \le 11$, $-21 \le l \le 21$ | $-10 \le h \le 10$, $-11 \le k \le 11$, $-22 \le l \le 22$ |
| no. of reflns collected/unique | 7772/4204 [$R_{int}$ = 0.054] | 16113/4993 [$R_{int}$ = 0.050] | 19574/5548 [$R_{int}$ = 0.057] |
| refinement method | full-matrix least-squares on $F^2$ | full-matrix least-squares on $F^2$ | full-matrix least-squares on $F^2$ |
| data/restraints/params | 4204/0/267 | 4993/0/328 | 5548/0/334 |
| GOF on $F^2$ | 0.925 | 1.11 | 1.10 |
| final $R$ indices [$I > 2\sigma(I)$] | $R$ = 0.048, $wR$ = 0.066 | $R$ = 0.070, $wR$ = 0.141 | $R$ = 0.086, $wR$ = 0.200 |
| $R$ indices (all data) | $R$ = 0.106, $wR$ = 0.075 | $R$ = 0.095, $wR$ = 0.150 | $R$ = 0.112, $wR$ = 0.212 |
| largest diff. peak and hole (e Å$^{-3}$) | 0.45 and −0.42 | 0.80 and −0.54 | 1.36 and −0.58 |

**X-ray Structure Determination of [2]$^+$ and [3]$^+$.** The crystals were sealed in a glass capillary under nitrogen stream. X-ray data were collected on a Nonius KappaCCD diffractometer. Diffractometer control program Collect,[14] unit cell parameters and data reduction with Denzo and Scalepak,[15] structure solved by direct methods SHELXS-97 [16] and refined on $F^2$ by full-matrix least-squares with SHELXL-97.[17] All the hydrogen atoms were placed in calculated positions and refined using a riding model. Crystal data, data collection, and refinement parameters for complexes **[2]**$^+$ and **[3]**$^+$ are given in Table 1.

## Result and Discussion

**Synthesis and Structure of 2, [2]$^+$, [3]$^+$.** Complex **2** was synthesized from 9-nickelafluorenyllithium **1** and (acetylacetonate)(pentamethylcyclopentadienyl)cobalt (58% yield) in diethyl ether, Scheme 2.

EIMS spectrum of **2** showed the parent ion at $m/e$ 469 ($^{58}$Ni calc.d) with an isotopic pattern characteristic for one nickel atom in the molecule. Because the magnetic moment of the analogue in which the Cp ring of the basal Ni atom is monomethylated in toluene solution at 294 K is 1.68 $\mu_B$, we confidently assume that also **2** has one unpaired electron.

Crystals of **2** appropriate for X-ray diffraction studies were obtained from hexane/dichloromethane solution. The molecular structure of **2** is presented in Figure 1.

The Ni−Co bond length (2.463(2) Å) is within the range of single bond. Four carbon atoms (C1, C2, C3, C4) and a nickel atom form a five-membered nickelacyclic ring. This

**Scheme 2**

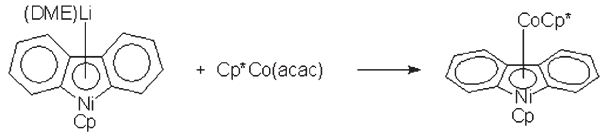


**1** **2**

ring is not planar. Four carbon atoms are situated in one plane, whereas the nickel atom deviates by 0.321 Å from this plane. The hinge angle, defined as the dihedral angle between the planes (C1, C2, C3, C4) and (C1, Ni, C4), is 13°. The cobalt atom is bonded to the two rings: one cyclopentadienyl and one nickelafluorenyl. The dihedral angle between the planes including those rings is 4.4°. To define a bonding mode of the central cobalt atom (Co) to the nickelafluorenyl ring, we have determined the degree of slip-fold distortion, using parameters as described in ref 18. The slip parameter, defined as $\Delta_{M\text{-}C}$ = avg $d$(Co−C1, Co−C7) − avg $d$(Co−C2, Co−C12), is 0.093 Å. This value shows that the coordination mode of the nickelacyclic ring to the cobalt atom is $\eta^5$.

On the basis of the the below described electrochemical findings, compounds **2** and **3** were oxidized chemically by $[Cp_2Fe]^+PF_6^-$ to form the corresponding monocations **[2]**$^+$ and **[3]**$^+$, Schemes 3 and 4, respectively.

Compound **2** reacted with $[Cp_2Fe]^+PF_6^-$ in dichloromethane to give dark-green solid compound **[2]**$^+$ (59% yield). Contrary to **2**, complex **[2]**$^+$ is diamagnetic. In the $^1$H NMR spectrum of **[2]**$^+$, there are resonances at 7.38−8.17, 5.56, and 1.31 ppm. Crystals of **[2]**$^+$ appropriate for X-ray diffraction studies were obtained from diethyl ether/dichloromethane solution. The compound crystallizes in the triclinic crystal system. Crystal data, data collection,

(14) *Collect Data Collection Software*; Nonius B. V.: Delft, The Netherlands, 1998.

(15) Otwinowski, Z.; Minor, W. Processing of X-ray Diffraction Data Collected in Oscillation Mode. In *Methods in Enzymology: Macromolecular Crystallography, Part A*; Carter, C. W. Jr., Sweet, R. M., Eds.; Academic Press: New York, 1997; Vol. 276, pp 307−326.

(16) Sheldrick, G. M. SHELXS-97; *Acta Crystallogr., Sect. A* 1990, 46, 467.

(17) Sheldrick, G. M. , *SHELXL-97, Program for the Refinement of Crystal Structures*; University of Göttingen: Göttingen, Germany, 1997.

(18) Westcott, S. A.; Kakkar, A. K.; Stringer, G.; Taylor, N. J.; Marder, T. B. *J. Organomet. Chem.* **1990**, *394*, 777.

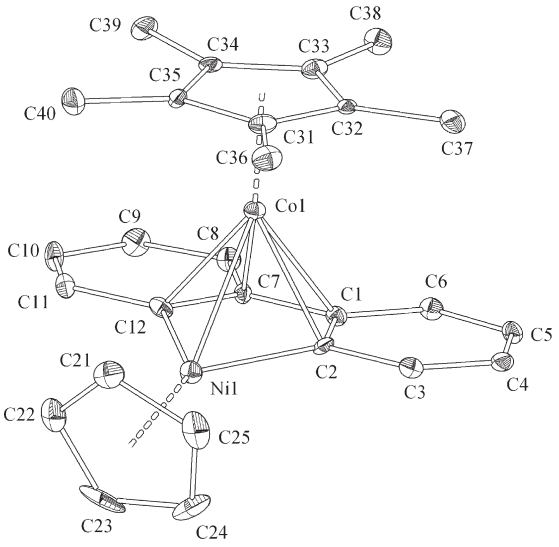


**Figure 1.** ORTEP view of the molecular structure of **2** showing the atom numbering scheme. Thermal ellipsoids drawn at the 30% probability level. Selected interatomic distances (Å) and angles (deg): Co1−Ni1 2.463 (2), Co1−C12 2.069(4), Co1−C2 2.077(4), Co1−C7 2.158(4), Co1−C1 2.174(4), Ni1−C12 1.904(4), Ni1−C2 1.907(4), C1−C2 1.438(5), C1−C7 1.456(5), C7−C12 1.431(5), C12−Ni1−C2 83.4(2), C12−Co1−C2 75.4 (2), Cg−Ni1−Co1 149.05(6), Cg−Co1−Ni1 139.48(6) (from hereafter: Cg = geometrical center of the Cp ring).

**Scheme 3**

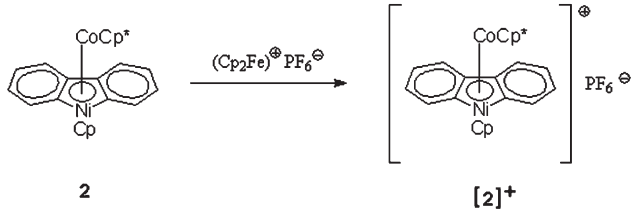


**Scheme 4**

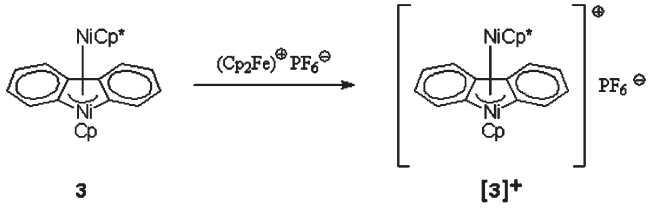


and refinement parameters are given in Table 1. The molecular structure of $[\mathbf{2}]^+$, which is illustrated in Figure 2, is similar to that of the neutral parent **2**.

The striking feature is the substantial shortening of the Co−Ni bond length, which in the case of $[\mathbf{2}]^+$ is 2.39 Å, 0.07 Å shorter than in **2**. The other bonds of **2** and $[\mathbf{2}]^+$ differ by no more than 2 ESDs. The slip parameter of Co atom in $[\mathbf{2}]^+$, defined as $\Delta_{M\text{-}C}$ = avg *d*(Co−C6, Co−C7) − avg *d*(Co−C1, Co−C12), is 0.068 Å, which is less than the slip parameter of Co atom in **2**. This value shows that the coordination mode of the nickelacyclic ring to the cobalt atom in $[\mathbf{2}]^+$ is $\eta^5$.

Compound **3** reacted with $[Cp_2Fe]^+PF_6^-$ in dichloromethane to give dark solid compound $[\mathbf{3}]^+$ (74% yield). Complex $[\mathbf{3}]^+$ is paramagnetic, but contrary to **3**, it does yield a $^1$H NMR spectrum of good quality. There are six

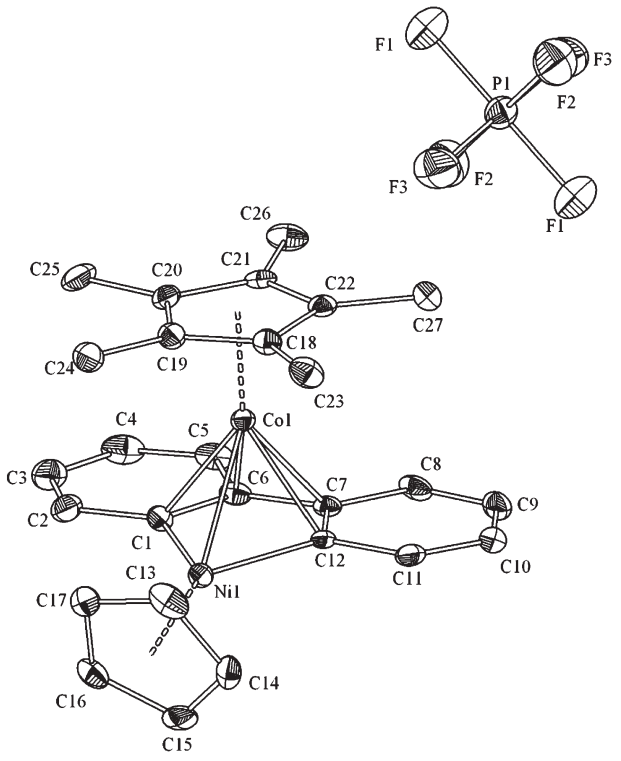


**Figure 2.** ORTEP view of the molecular structure of $[\mathbf{2}]^+$ showing the atom numbering scheme. Thermal ellipsoids drawn at the 30% probability level. Selected interatomic distances (Å) and angles (deg): Co1−Ni1 2.387(1), C1−C6 1.436(8), C6−C7 1.449(8), C7−C12 1.428(8), C1−Ni1 1.902(6), C12−Ni1 1.907(5), C1−Co1 2.072(6), C6−Co1 2.130(5), C7−Co1 2.131(5), C12−Co1 2.051(5), C1−Co1−C12 77.0(2), C1−Ni1−C12 84.8(2), Cg−Ni1−Co1 151.19(4), Cg−Co1−Ni1 138.15(4).

resonances at 96.26, 10.35, 1.71, −1.21, −4.56, −19.00, and −23.63 ppm.

Crystals of $[\mathbf{3}]^+$ appropriate for X-ray diffraction studies were obtained from diethyl ether/dichloromethane solution. Crystal data, data collection, and refinement parameters are given in Table 1. The compound crystallizes in the triclinic crystal system. The molecular structure of $[\mathbf{3}]^+$ is presented in Figure 3.

Also in this case, the molecular structure of the cation is similar to the structure of the neutral parent **3**.[7] The striking feature is the substantial shortening of the Ni1−carbon (C1, C6, C7) bond lengths in $[\mathbf{3}]^+$. The Ni1−C6 bond length in $[\mathbf{3}]^+$ is shorter than the corresponding bond length in **3** by 0.20 Å, and the Ni1−C7 bond length in $[\mathbf{3}]^+$ is shorter than the corresponding bond length in **3** by 0.16 Å. The substantial shortening of Ni1−C6 and Ni1−C7 bond lengths causes the decrease in the value of the slip parameter of Ni1 atom in $[\mathbf{3}]^+$. The slip parameter of Ni1 atom in $[\mathbf{3}]^+$ defined as $\Delta_{M\text{-}C}$ = avg *d*(Ni1−C6, Ni1−C7) − avg *d*(Ni1−C1, Ni1−C12) is 0.083 Å, which is much less (0.133 Å) than the slip parameter of Ni1 atom in **3.** This value shows that the coordination mode of the nickelacyclic ring to the Ni1 atom in $[\mathbf{3}]^+$ is $\eta^5$ contrary to **3**, where the coordination mode was between $\eta^3$ and $\eta^5$.

**Electrochemistry.** As illustrated in Figure 4, complex **3** undergoes in THF solution two oxidations and one reduction, all having features of chemical reversibility but electrochemical quasireversibility in the cyclic voltammetric time scale. Because complex **3**, even in

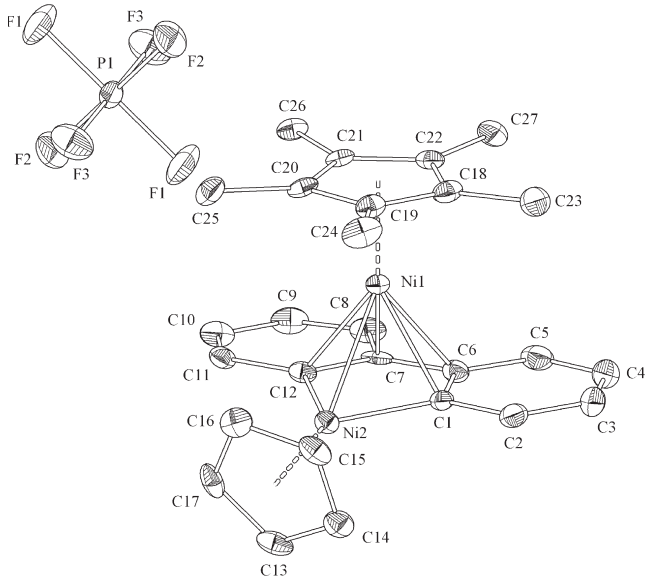


**Figure 3.** ORTEP view of the molecular structure of $[\mathbf{3}]^+$ showing the atom numbering scheme. Thermal ellipsoids drawn at the 30% probability level. Selected interatomic distances (Å) and angles (deg): Ni1−Ni2 2.402(1), C1−C6 1.422(9), C6−C7 1.447(10), C7−C12 1.444(9), C1−Ni1 2.100(6), C6−Ni1 2.180(7), C7−Ni1 2.212(7), C12−Ni1 2.127(6), C1−Ni2 1.903(6), C12−Ni2 1.916(6), C1−Ni1−C12 74.9(2), C1−Ni2−C12 84.6(3), Cg−Ni2−Ni1 147.55(4), Cg−Ni1−Ni2 140.38(5).

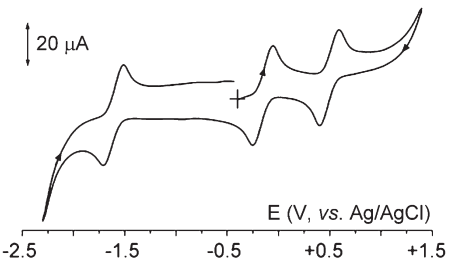


**Figure 4.** Cyclic voltammogram recorded at a platinum electrode in THF solution of **3** ($2.3 \times 10^{-3}$ mol dm$^{-3}$). $[NBu_4][PF_6]$ (0.2 mol dm$^{-3}$) supporting electrolyte. Scan rate: 0.2 V s$^{-1}$. $T = 253$ K.

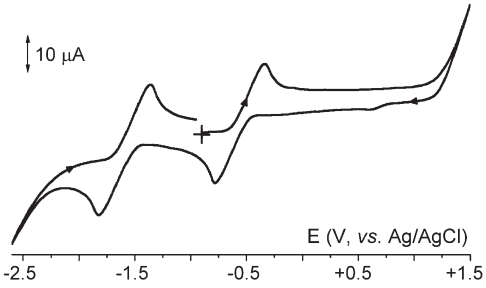


**Figure 5.** Cyclic voltammogram recorded at a platinum electrode in THF solution of **2** ($2.9 \times 10^{-3}$ mol dm$^{-3}$). $[NBu_4][PF_6]$ (0.2 mol dm$^{-3}$) supporting electrolyte. Scan rate: 0.2 V s$^{-1}$. $T = 253$ K.

deareated solution, tends to oxidize rather quickly (the solution progressively changes from red-brown to deep brown), it is undoubted that the first anodic oxidation involves a one-electron process, in that the chemically isolated monocation $[\mathbf{3}]^+$ displays a quite complementary cyclic voltammetric profile (see Figure S1 in the Supporting Information). In this connection, analysis of the cyclic voltammetric response of the first oxidation process with scan rates varying from 0.02 V s$^{-1}$ to 2.00 V s$^{-1}$ shows that (i) the ratio $i_{p(reverse)}/i_{p(direct)}$ is constantly equal to the unity; (ii) the current function $i_p\, v^{-1/2}$ remains substantially constant; (iii) the peak-to-peak separation is significantly higher with respect to the theoretical value of about 60 mV expected for an electrochemically reversible one-electron process and it tends to increase with the scan rate.[9] The same trend substantially holds for the other redox processes.

It is noted that such a behavior is quite reminiscent of that exhibited by the permethylated analogue previously studied.[3]

As far as the redox behavior of complex **2** is concerned, the replacement of the nickel ion for the cobalt ion causes significant changes in the redox activity. In fact, as shown in Figure 5, the complex exhibits only one oxidation and one reduction, with both the coulometrically measured one-electron processes having features of chemical reversibility in the cyclic voltammetric time scale.

The electrode potentials of the different redox changes exhibited by complexes **2** and **3** are reported in Table 2.

**Extended Hückel Calculation.** As mentioned, we have previously reported an extended Huckel study[3] on the electronic structure of nickelocene analogues of **3** by using simplified models in which the substituents of the nickelacycle ring have been replaced by hydrogen atoms. The results indicated that, given the asymmetry of the system, the relative frontier molecular orbitals were sequentially localized or delocalized. As a consequence, the description of this kind of complexes through fractional oxidation states has revealed to be more suitable to describe their electronic structure.

In fact, the $\{Ni_2\}^{4+}$ system was better represented as $Ni^{2.5+}_{apical}Ni^{1.5+}_{basal}$, where "apical" indicates the sandwiched ion and "basal" indicates the nickel ion in the ring. As expected, a similar pattern is obtained for complex **3** and **2**, even if in this case we modeled the complete nickelafluorenyl ring. In Figure 6, the three frontier orbitals required for the following discussion are shown, whereas the contribution of the metal ions to each molecular orbital is reported in Table 3.

To better compare the homo- (**3**) and heteronuclear (**2**) complexes and explain their redox behavior, it is convenient to consider isoelectronic systems: therefore, the redox activity of **3** should be compared with that of $\mathbf{2}^-$. The nature of the sandwiched metal has a relevant effect, because the removal of the first and second electron results much more favored in $\mathbf{2}^-$ than in **3** ($E^{\circ\prime}_{[\mathbf{2}]^-/\mathbf{2}} = -1.53$ V, vs $E^{\circ\prime}_{\mathbf{3}/[\mathbf{3}]^+} = -0.03$ V and $E^{\circ\prime}_{\mathbf{2}/[\mathbf{2}]^+} = -0.57$ V, vs $E^{\circ\prime}_{\mathbf{3}/[\mathbf{3}]^+} = +0.61$ V). As summarized in Figure 7, a similar trend is observed for the redox values of the isolectronic $[CoCp_2]^-$ and $NiCp_2$ metallocenes, and in this case, the shift is even more relevant.

The molecular charge and the orbital energies may both contribute to the redox potential shift observed changing Ni for Co; nevertheless, as shown in Figure 8, it is possible to obtain a good quality linear fit between the latter and the redox potential values, which is indicative of the main role of the orbital energies.

To conclude, the present semiempirical calculations also explain the structural modifications occurring as a consequence of the electron removal. Indeed, in the cation $[\mathbf{2}]^+$, the Co−Ni bond length is shorter than that observed in the neutral complex **2** (2.387 Å vs 2.463 Å, $\Delta = 0.076$ Å), and in fact the formation of $[\mathbf{2}]^+$ involves

**Table 2.** Formal Electrode Potentials (V, vs Ag/AgCl), peak-to-peak separations (mV) (in parentheses; measured at 0.2 V $s^{-1}$), and current ratios (measured at 0.2 V $s^{-1}$) for the redox changes of complexes **2** and **3** in THF solution at 253 K.

| complex | $E^{o\prime}$ (2nd ox) | $i_{p(b)}/i_{p(f)}$ | $E^{o\prime}$(1st ox) | $i_{p(b)}/i_{p(f)}$ | $E^{o\prime}$ (1st red) | $i_{p(b)}/i_{p(f)}$ | ref |
|---|---|---|---|---|---|---|---|
| **2** | | | −0.57 (182) | 1.0 | −1.53 (192) | 0.8 | this work |
| **3** | +0.61 (211) | 1.0 | −0.03 (144) | 1.0 | −1.51 (193) | 0.9 | this work |
| $CoCp_2$ | | | −0.85 | | −1.99 | | 19 |
| $NiCp_2$ | +1.01 (132) | 0.8 | +0.17 (136) | 1.0 | −1.77(145) | 0.4 | 3 |

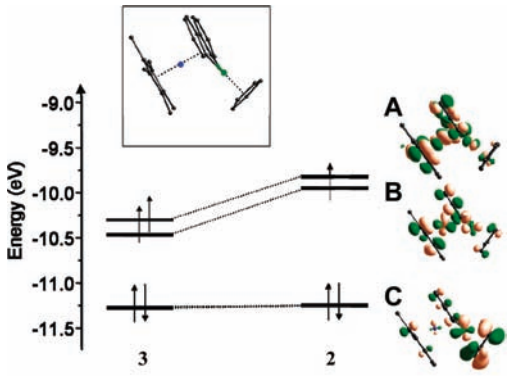


**Figure 6.** Frontier orbitals of complex **2** (right) and **3** (left).

**Table 3.** Apical/Basal Metal Ion Contribution to the Frontier Orbitals of **2** and **3**

| | **2** | | **3** | |
|---|---|---|---|---|
| MO | $Co_{apical}$ (%) | $Ni_{basal}$ (%) | $Ni_{apical}$ (%) | $Ni_{basal}$ (%) |
| A | 23 | 5 | 21 | 3 |
| B | 23 | 11 | 21 | 10 |
| C | 4 | 18 | 2 | 21 |

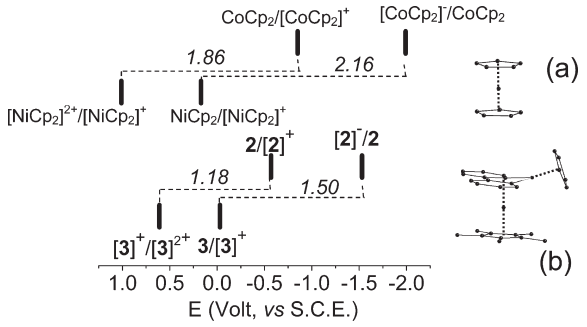


**Figure 7.** Comparison between the redox potential values of (a) cobaltocene/nickelacene and (b) **2**/**3**.

the removal of one electron from the orbital **B** arising from the antibonding interaction between the cobalt and the nickel ions. In contrast, in the cation $[\mathbf{3}]^+$, the Ni−Ni bond length remains substantially unchanged (2.402 Å vs 2.397 Å, $\Delta$ = 0.005 Å), and in fact, its formation is a consequence of the removal of one electron from the orbital **A** mainly centered on the apical nickel.

**EPR Spectroscopy.** To throw further light on the nature of the above-discussed redox processes, EPR measurements have been carried out either on the original complexes **2** and **3** or in their electrogenerated redox congeners.

In THF solution, complex **3**, in agreement with its solid-state magnetic moment $\mu_B$ = 3.084 (at 293 K), which preludes the presence of two unpaired electrons

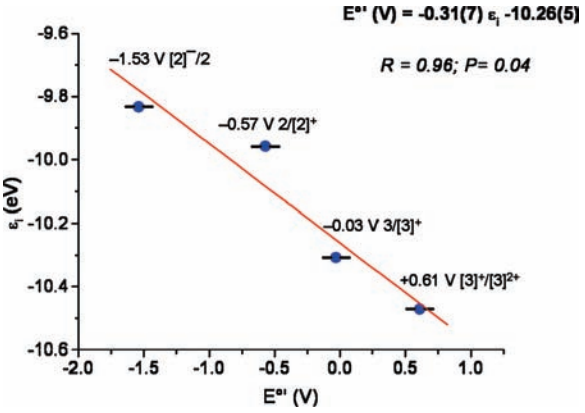


**Figure 8.** Linear fit between the formal electrode potentials vs. the orbital energies ($\varepsilon_i$) of **2** and **3**.

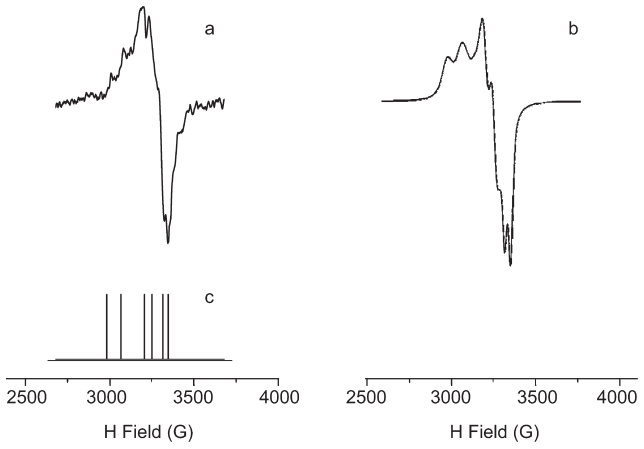


**Figure 9.** X-band EPR spectra of a THF solution of **3**: (a) experimental first derivative spectrum; (b) simulated first derivative spectrum; (c) stick diagram. $T$ = 10 K. Operational frequency $\nu$ = 9.39 GHz.

(total electron spin S = 1 in the ground state) is EPR-active, Figure 9.

The broad rhombic line shape has been interpreted according to the electron spin Hamiltonian: $H_e = \beta HgS + SDS$ ($\beta HgS$, Zeeman contribution; $SDS$, zero-field splitting contribution; $D$, traceless zero-field splitting tensor (ZFS)).[20,21,22]

In the low-field region, two partially resolved doublets ($g_l$, $g_m$) are present, which give the evidence for active zero-field splitting interactions. Concomitantly, the high-field zone exhibits a less-resolved doublet that is due to the

(19) Bard, A. J.; Garcia, E.; Kukharenko, S.; Strelets, V. V. *Inorg. Chem.* **1993**, *32*, 3528.
(20) Mabbs, F. E.; Collison, D. Electron Paramagnetic Resonance of d Transition Metal Compounds. In *Studies in Inorganic Chemistry*; Elsevier: New York, 1992; Vol. 16.
(21) Drago R. S. *Physical Methods for Chemists*; Saunders College Publishing: New York, 1992.
(22) Carlin R. L. *Magnetochemistry*; Springer-Verlag: Berlin, 1986.

**Table 4.** Calculated X-Band EPR Parameters of the Paramagnetic Species Examined[a]

| complex | $g_l$ | $g_m$ | $g_h$ | $\langle g \rangle$ | $D_l$ | $D_m$ | $D_h$ | $a_l$ | $a_m$ | $a_h$ | $\langle a \rangle$ | $\Delta H_l$ | $\Delta H_m$ | $\Delta H_h$ | $\Delta g_{l-h}$ |
|---|---|---|---|---|---|---|---|---|---|---|---|---|---|---|---|
| **3**[b] | 2.216 | 2.070 | 2.003 | 2.096 | 89 | 50 | 35 | | | | | 28.0 | 16.0 | 11.5 | 0.213 |
| **[3]**$^{+}$[b] | 2.051 | 1.992 | 1.856 | 1.966 | | | | | | | | 22 | 19 | 38 | 0.195 |
| **2**[c] | 2.050 | 1.990 | 1.990 | 2.010 | | | | 75 | $< \Delta H_m$ | 30 | $< 43$ | 35 | 25 | 35 | 0.060 |
| **2**[b] | 2.099 | 1.990 | 1.970 | 2.020 | | | | $< 100$ | $< 5$ | $< 90$ | $< 65$ | 9 | 9 | 12 | 0.129 |

[a] $T = 10$ K. $\delta g_{l-h} = g_l - g_h$. Low-field, l; medium-field, m; high-field, h; $g_i$, $\pm 0.008$; $D_i$, $\pm 3$ G; $a_i$, $\pm 6$ G; $\Delta H_i$, $\pm 4$ G; $\delta g_{l-h}$, $\pm 0.008$; $\langle g \rangle = (g_l + g_m + g_h)/3$; $D_i$, $a_i$, $\Delta H_i$ in Gauss. [b] In THF solution. [c] In the solid state.

relevant minor ZFS coupling. The parent stick diagram (Figure 9c) accounts for the decreasing of the experimental ZFS separation with the $H$ magnetic field.

Accordingly, the anisotropic $g_i$ and $D_i$ parameters have been evaluated by multiple derivative line shape analysis (first and third derivative) joined with simulation procedures, and they are reported in Table 4, together with those of the remaining paramagnetic derivatives.

The pertinent $g_i$ and $D_i$ values clearly prove the metallic character imparted by the strong Ni spin−orbit coupling.[19,20] No EPR evidence for hyperfine (hpf) $^{61}$Ni ($I = 3/2$, natural abundance = 1.19%) or superhyperfine (shpf) $^{13}$C aromatic ligand interaction is detected, in that the experimental signal is significantly noised and the relevant $^{61}$Ni and $^{13}$C natural abundances are very low. By comparison, the calculated $\mu_{eff} = 2.96 \pm 0.03$, at 10 K, agree well with the mentioned value measured in the solid state at room temperature. On the other hand, the theoretical value expected under the $S = 1$ "spin only" approximation very closely fits our experimental data.

The EPR features of the electrogenerated monocation **[3]**$^{+}$ are typical of a metallic complex with $S = 1/2$, having rhombic symmetry partially resolved in $g_i$ parameters, Figure 10.

The rhombic symmetry of the relatively narrow line shape ($g_i \neq g_e = 2.0023$) gives evidence to some metallic character of the unpaired electron. The $g_{l,m,h}$ features (see Table 4) well-account for the metal spin−orbit coupling contribution to the anisotropic signals.

Again, no hyperfine (hpf) $^{61}$Ni or superhyperfine (shpf) $^{13}$C aromatic ligand coupling is detected. The calculated $\mu_{eff} = 1.70 \pm 0.03$, at 10 K, once again well fits the "spin only" value.

It is noted that complex **3** looks like to exhibit a more metallic character than the corresponding **[3]**$^{+}$, as it results from the related $g_i$ and $\delta g_{l-h}$ and $\mu_{eff}$ parameters.

As expected, the present features are similar to those of the previously reported nickelanickelocene analogue.[3]

Figure 11 shows the X-band EPR spectra of the paramagnetic complex **2** in THF solution. The liquid helium temperature spectrum shows the hyperfine coupling with $^{59}$Co ($I = 7/2$).

The spectrum has rhombic symmetry and suggests an high contribution of 3d Co orbitals to the SOMO. The low- and high-field spectral regions ($g_l$ and $g_h$) are partially resolved, whereas the medium-field one is substantially unresolved (interestingly, there is the presence of some byproduct species, the features of which are metal in nature, the spectral intensity of which increases with the proceeding of the exhaustive oxidation; $g_\perp = 2.002 \pm 0.002$, $g_{||} = 2.029 \pm 0.003$). The $\mu_{eff}$ of 1.75 $\mu_B$ calculated from the $\langle g \rangle$ values is close to the theoretical value obtained with the spin-only approximation (1.73) and in good agreement with the relevant value of cobaltocene (1.76 $\mu_B$).[23]

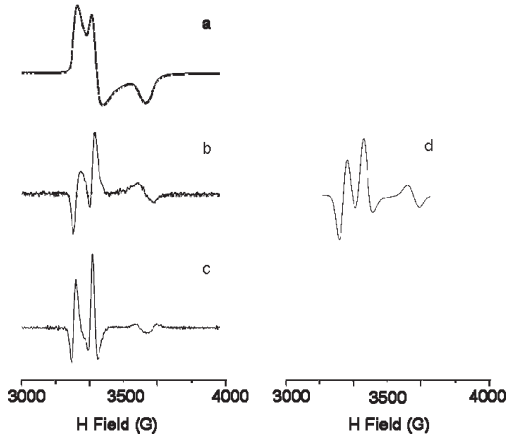


**Figure 10.** X-band EPR spectra of a THF solution of **[3]**$^{+}$: (a) experimental first derivative spectrum; (b) experimental second derivative spectrum; (c) experimental third derivate spectrum; (d) simulated second derivate spectrum. $T = 10$ K. Operational frequency $\nu = 9.39$ GHz.

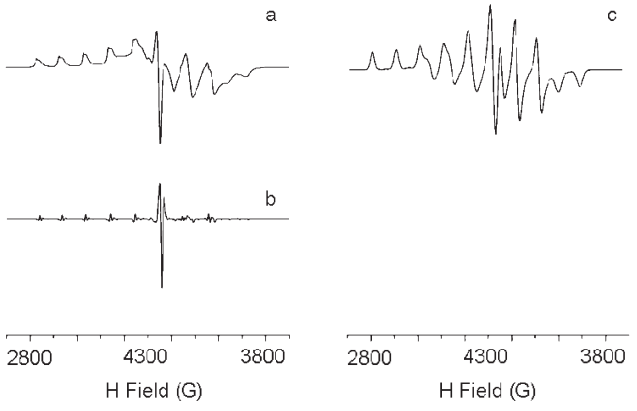


**Figure 11.** X-band EPR spectra of a THF solution of **2**: (a) experimental first derivative spectrum; (b) experimental third derivative spectrum; (c) simulated first derivative spectrum. $T = 10$ K. Operational frequency $\nu = 9.39$ GHz.

The multiple derivative line shape analysis and simulation procedures have been carried out in terms of the $S = 1/2$ anisotropic Zeeman Hamiltonian, with $g_{l,m,h}$ values significantly different from 2.0023 (see Table 4). They point out the metallic character of the SOMO. No $^{61}$Ni, or $^{13}$C couplings are detected.

It is noted the appearance of two very similar rhombic spectra, substantially superimposed each other, but recognizable in multiple derivative analysis as resulting from a light doubling of the signals (i.e., with slightly different values of the corresponding $g_i$ and $a_i$ values), Figure 11b. The relevant spectra suggest the contemporary

(23) Retting, M. F.; Drago, R. S. *J. Am. Chem. Soc.* **1969**, *91*, 1361.

presence of two $^{59}$Co complexes with slightly differences in the coordination geometry, likely coming out from the different positions of the pentamethycyclopentadienyl ligand with respect to the nickelafluorenyl ring.[24] In agreement with the significantly broad experimental line shape, the two $^{59}$Co geometrical isomers are in about a 3:1 molar ratio. Interestingly, the $g_l$, $g_h$, and $\delta g_{l-h}$ values of **2** in the solid state and glassy solution are quite different. Such a magnetic behavior is likely due to important spin−spin interactions in the solid state and concomitant cell constriction.

## Conclusions

Recently, we have shown that 9-nickelafluorenyllithium can act as a donor of nickelafluorenyl ring in the reactions with metal salts where diheterometallocenes are formed.[5] In the present paper, we have expanded the use of 9-nickelafluorenyllithium in the synthesis of the monoheterometallocene **2**. In spite of apparently similar structural features, complexes **2** and **3** exhibit rather different electrochemical behavior.

On the basis of the electrochemical findings, we have oxidized chemically complexes **2** and **3** to their cations $[\mathbf{2}]^+$ and $[\mathbf{3}]^+$. The structural slip parameters of such cations are lower than in their neutral precursors **2** and **3**, thus suggesting that the pertinent electron removals reinforce the interaction between the central metal atom and the nickelafluorenyl ring.

The paramagnetic members of the couples $\mathbf{2}/[\mathbf{2}]^+$ and $\mathbf{3}/[\mathbf{3}]^+$ have been characterized by EPR techniques, together with their $\mu_{eff}$ calculations.

On the basis of EH theoretical studies, the molecular orbitals of the $\mathbf{2}/[\mathbf{2}]^+$ and $\mathbf{3}/[\mathbf{3}]^+$ couples are localized or delocalized depending on their interaction with the $\pi$-system of the 9-nickelafluorenyl ring. The SOMO higher in energy is mainly localized on the apical ion, whereas the SOMO lower in energy is a strong mixing between the orbitals $d_{yz}$ of the two metallic ions.

**Acknowledgment.** P.Z. gratefully acknowledges the financial support of the University of Siena (PAR2007).

PB acknowledges the financial support of the Polish Ministry of Education and Science (Grant N N204 237234).

**Supporting Information Available:** Cyclic voltammogram (PDF). This material is available free of charge via the Internet at http://pubs.acs.org.

(24) Schneider, J. J.; Czap, N.; Spickermnn, D.; Lehmann, W.; Fontani, M.; Laschi, F.; Zanello, P. *J. Organomet. Chem.* **1999**, *590*, 7–14.